Nonlinear Dynamics in Optical Systems,
OSA Proceedings, vol. 7,
N. B. Abraham, E. M. Garmire, and P. Mandell, eds.
(Optical Society of America,
Washington, DC, 1990) pp. 504-508.

Amplification, Instability, and Chaos in Nonlinear Counterpropagating Waves

C. T. Law and A. E. Kaplan

Department of Electrical and Computer Engineering,
Johns Hopkins University, Baltimore, Maryland 21218

Abstract

We demonstrate that two linearly polarized counterpropagating waves in a Kerr nonlinear medium with linear dispersion can exhibit amplification and multi-mode temporal instability, which are attributed to the combined effect of nonlinear index grating and linear dispersion.

1. Introduction

The cross-interaction of two counterpropagating laser beams [1]-[6] in a third order nonlinear material is a conceptionally simple and fundamental process in nonlinear optics. The steady states of this interaction have been shown to exhibit various interesting and complicated features. Earlier theoretical investigations have demonstrated the existence of temporal instability and chaos under various extensions of this system, in particular, for a nonlinear medium having finite relaxation time [6]. However, the relaxation of nonlinear refractive index may not be the most likely mechanism of instability of beam intensity in most of the nonlinear systems since it imposes too stringent requirements on relaxation time.

Recently, we showed [7] that another physical factor, namely regular linear dispersion (i.e. frequency dependence of refractive index) can be a natural and universal agent for amplification of perturbations and temporal instability in the counterpropagating nonlinear waves. In this paper, we present the study of the effect and also explore its possible use for large broad-band amplification that may exist in the system if the pumping is below the threshold of instability. It is well known that linear dispersion can give rise to nonlinear optical effects such as spatial instability of single plane wave [8], formation of soliton in nonlinear fiber [9], and amplification of copropagating waves [10]. This suggests that linear dispersion in combination with nonlinear processes can dramatically change the dynamical behavior of a system.

2. Wave equations

In order to demonstrate the instability effect, we investigate the simplest spatially stable eigenpolarization [2,3] whereby the two waves are linearly polarized with electrical fields parallel to each other. (Spatial stability of the eigenpolarization is essential since spatially unstable polarization arrangements may result in temporal instability even if no other mechanism is present [11].)

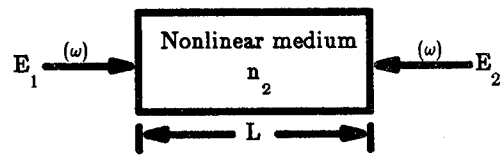

Figure 1. Counterpropagating waves in a Kerr nonlinear medium.

For the configuration shown in Fig. 1, the total complex electric field of the two counterpropagating plane waves in the Kerr nonlinear medium is represented as: $\vec{E} = [E_1(z,t)e^{ikz} + E_2(z,t)e^{-ikz}]\, e^{-i\omega t}\hat{e}_x$ where $E_1(z,t)$ and $E_2(z,t)$ are the slowly varying envelopes of forward (+z) and backward (-z) propagating waves respectively. The dynamics of these envelopes is governed by two coupled nonlinear Schrodinger equations [7]:

$$i\left((-1)^{j+1}\frac{\partial E_j}{\partial z} + \frac{1}{v_g}\frac{\partial E_j}{\partial t}\right) - \frac{\mu}{2}\frac{\partial^2 E_j}{\partial t^2} = -\beta(2I_{3-j} + I_j)E_j\ ;\ j = 1, 2 \qquad (1)$$

where $I_j = |E_j|^2$ is the intensity of the respective propagating wave, $\mu = \partial^2 k/\partial\omega^2$ is the linear dispersion parameter, $\beta = n_2 k/n$ is the nonlinear parameter, n is the linear refractive index at the frequency ω, v_g is the linear group velocity, n_2 is the nonlinear refractive index coefficient, and k is the wave number in the medium. The coefficient 2 in the right-hand side in Eq. (1) reflects light-induced nonreciprocity [12]. The problem of temporal instability of cw wave propagation for certain signs of dispersion and nonlinearity is isomorphic to the problem of cross-induced self-focusing bistability [13] and spatial instability of plane counterpropagating waves in nonlinear medium [14], since the latter problem can be described by Eq. (1) in which the term with $\partial^2 E/\partial t^2$ is replaced by $\partial^2 E/\partial x^2$ where x is an coordinate in the transverse plane (i.e. spatial dispersion).

3. Instability

To analyze the small perturbation stability of the steady state, we represent both waves in the system as slightly perturbed steady state in the form:

$$E_j = E_{j0}(\xi)[1 + A_{1,j}(\xi)e^{\lambda\tau} + A^*_{2,j}(\xi)e^{\lambda^*\tau}] \quad (2)$$

where $j=1,2$, E_{j0} is the steady solution for Eq. (1), $A_{1,j}$ and $A_{2,j}$ are normalized amplitude of the small perturbations, $\tau = tv_g/L$ is the normalized time, and $\xi = z/L$ is the normalized distance of propagation. Substituting Eq. (2) into Eq. (1) and linearizing the latter equation, we obtain four linear propagation equations for $A_{k,j}$:

$$\frac{dA_{k,j}}{d\xi} = i(-1)^{k+j}\Big\{A_{k,j}[p_j - i(-1)^k\lambda - d\lambda^2] + p_j A_{3-k,j} + 2p_{3-j}(A_{1,3-j} + A_{2,3-j})\Big\}; \quad j,\ k = 1,2 \quad (3)$$

where $p_j = \beta I_{j0} L$, $d = \mu v_g^2/(2L)$, and I_{j0} is the intensity of each wave. Here p_j are the normalized pumping intensities of the two beams (note that p_j can have negative sign depending on nonlinearity β), and d is the normalized dispersion. At this point we simplify our calculation, assuming equal intensities of the waves, i.e. $I_{10} = I_{20} = I$. Using the boundary conditions for the perturbation amplitudes $A_{k,j}$ for $k = 1,2$ and $j = 1,2$:

$$A_{1,1}(\xi=0) = A_{1,2}(\xi=1) = A_{2,1}(\xi=0) = A_{2,2}(\xi=1) = 0,$$

one can obtain an equation for λ. The boundaries of unstable regions are found by setting $\mathrm{Re}(\lambda) = 0$ and solving for the normalized driving intensity $p = \beta IL$ and $\mathrm{Im}(\lambda)$ for a given dispersion.

The numerical results of this procedure are depicted in Fig. 2 which shows the normalized threshold intensity p_{cr} (>0) versus normalized dispersion d in a semi-log plot. The solid line is the ultimate (encompassing) boundary of instability. Above this boundary there are numerous solutions corresponding to various unstable modes of oscillation. As the dispersion decreases, the boundaries for individual modes are too closely packed together to be shown in Fig. 2. These individual boundaries correspond to the longitudinal modes in a light-induced, distributed-feedback resonator. Only a few of these solutions and the boundary encompassing all the unstable solutions (i.e. the solid line) are shown in Fig. 2. In the inset of Fig. 2, the number of unstable modes is plotted against $|p|/p_{cr}$ where $p_{cr} = 1.98$ is the threshold intensity for the case $|d| = 0.01$. One can see that when the pumping is only slightly above the threshold, only one mode become unstable, then two, and so on. When the number of modes is greater than one, they compete with each other and some of them can become dominant while others fade out.

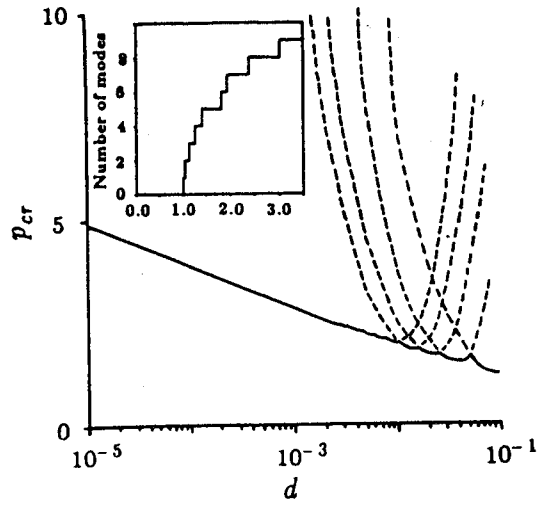

Figure 2. Normalized threshold intensity p_{cr} vs normalized dispersion d. The solid line is the boundary of instability above which the system is unstable. The dashed lines indicate boundaries of instability of individual modes. Inset: number of unstable modes versus $|p|/p_{cr}$ where p is normalized driving intensity for normalized dispersion $|d| = 0.01$.

The (encompassing) threshold intensity increases as dispersion decreases; our numerical calculations show that for sufficiently small $|d|$, this dependence can be best described by a surprisingly simple relationship

$$p_{cr} = -sgn(pd)\,|\log_\eta |d||| \quad (4)$$

where η is numerically determined to be $10.0 \pm 1\%$, and $\mathrm{sgn}(pd)$ is the sign of pd. The necessary condition for initiating instability (i.e. to have $p_{cr} > 0$) is that the signs of nonlinearity n_2 and dispersion μ must be opposite, which coincides with the necessary condition for formation of a soliton and spatial instability in single-wave propagation.

To explore the full dynamical behavior in unstable region showed in Fig. 2, we have numerically integrated Eq. (1) with the dispersion fixed at $|d| = 0.01$ (we choose this unrealistically large

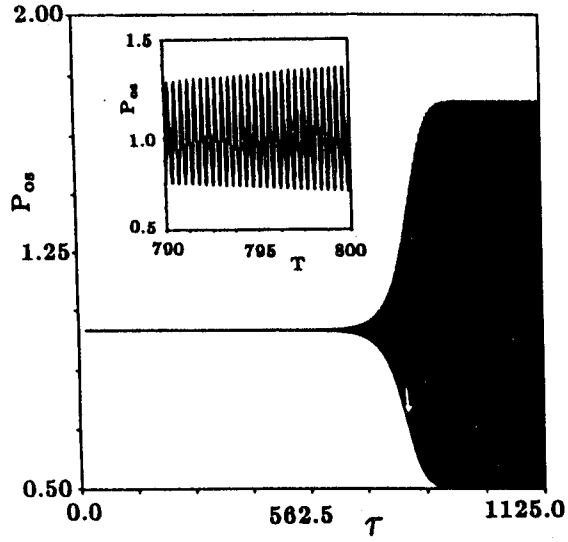

Figure 3. Normalized intensity p_{os} of oscillations versus the normalized time τ for a driving intensity $|p/p_{cr}|=1.02$ (single-mode oscillations; fixed normalized dispersion $|d|=0.01$ excitation with $p_{cr}=1.98$); the inset depicts the enlargement of the region indicated by an arrow and demonstrates single-mode nature of excitation. The frequency of oscillations is $\simeq 17.2\, v_g L^{-1}$.

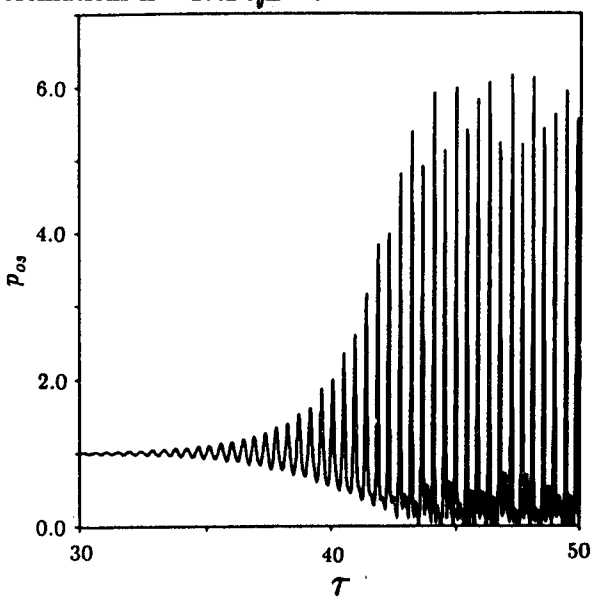

Figure 4. The same as in Fig. 3 except the driving intensity $|p/p_{cr}|=1.25$ (three unstable modes are engaged for $p_{cr}=1.98$); the excitation shows formation of subharmonic and onset of chaos. The initial frequency of oscillations is slightly less that the one shown in Fig. 3.

dispersion parameter for the sake of illustrating the appearance of new unstable modes). The slow increase of intensity of oscillations, p_{os}, with τ when the intensity is slightly greater then the threshold ($|p/p_{cr}|=1.02$) is shown in Fig. 3. At such a pumping intensity, only one mode is unstable (see the inset in Fig. 2), and eventually develops into periodic self-sustained oscillations with a stable amplitude. When the value of $|p/p_{cr}|$ is further increased to 1.28, the instability and resulting self-sustained oscillations develop much faster as is shown in Fig. 4. In this case three modes satisfy the excitation condition (see the inset in Fig. 2); as the oscillations develop in time, the second subharmonic is excited which later evolves into aperiodic oscillations with randomly modulated amplitude and phase which indicates onset of chaos. We expect this behavior to further develop into strongly pronounced chaos when the pumping intensity is significantly higher than the threshold

In order to estimate the threshold intensity for instability, we consider an example of a 1 km long single-mode fiber with Ge-doped silica core at wavelength 1.55 μm with group velocity dispersion $D(k) = 6.5\times10^{-3}$ [note that $\mu=-D(k)/(kc^2)$] (the corresponding $d=-8.02\times10^{-13}$), refractive index $n = 1.44$, and $n_2=3.2\times10^{-16}\ cm^2/W$ [15], in the lossless approximation. We find the threshold intensity I_{cr}, Eq. (4), for such a fiber to be 9.3 MW/cm^2, which is below the damage threshold $10^{10}\ W/cm^2$ for fused scilica [16]. Crude estimate shows that the losses existing in the real fiber (~ 0.5 dB/km [15]) would require only about two times higher threshold intensity. If we use the SF-59 glass with $n_2=7\times10^{-15}\ cm^2/W$ [17] at wavelength 1.06 μm, and assume that n_2 at wavelength 1.55 μm is of the same order as that of 1.06 μm and that dispersion is roughly the same as for plain glass, the critical intensity is reduced to $\sim 425\ kW/cm^2$ for the same length.

4. Amplification

To find the gain spectrum of this system, we inject a weak probe beam into the nonlinear medium and scan the beam frequency. In Fig. 5, we show a new configuration with two pump beams and four weak beams. Suppose that the probe beam ($E_{10}A_{1,1}$) has frequency of $\Omega+\delta\Omega$, i.e. its frequency deviated from that of the pump beams with normalized frequency Ω by $+\delta\Omega$; then we expect a phase conjugate signal ($E_{20}A_{2,2}$) to be reflected back with frequency $\Omega-\delta\Omega$. These two beams are referred to as direct-coupled waves [18]. The remaining two weak beams are referred to as cross-coupled forward ($E_{10}A_{2,1}$) and backward ($E_{20}A_{1,2}$) waves with their frequencies equal to $\Omega-\delta\Omega$ and $\Omega+\delta\Omega$ respectively. Since we consider a collinear geometry, the effect of the cross-coupled waves cannot be neglected [18].

Since the only differences between perturbation in Section 3 and the four signal waves in here are that the boundary conditions for one of the signal waves (specifically, for a probe wave) is nonzero [$A_{2,1}(\xi=0)=A_{1,2}(\xi=1)=A_{2,2}(\xi=1)=0$, and $A_{1,1}(\xi=0)=C=const$] and the detuning frequency is set by the probe wave, we can treat $A_{1,1}$, $A_{2,1}$, $A_{1,2}$, and $A_{2,2}$ in here using the same procedure outlined in Section 3. The numerical results of solving Eq.

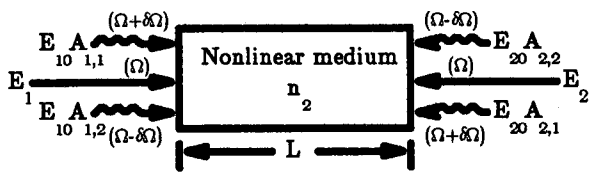

Figure 5. Pump-probe configuration for amplification measurement where E_1 and E_2 are pumping waves and $E_{10}A_{1,1}$ is the input probe wave with $E_{10}A_{2,1}$, $E_{20}A_{1,2}$ and $E_{20}A_{2,2}$ generated as a result of the wave mixing process.

(3) are shown in Fig. 6.

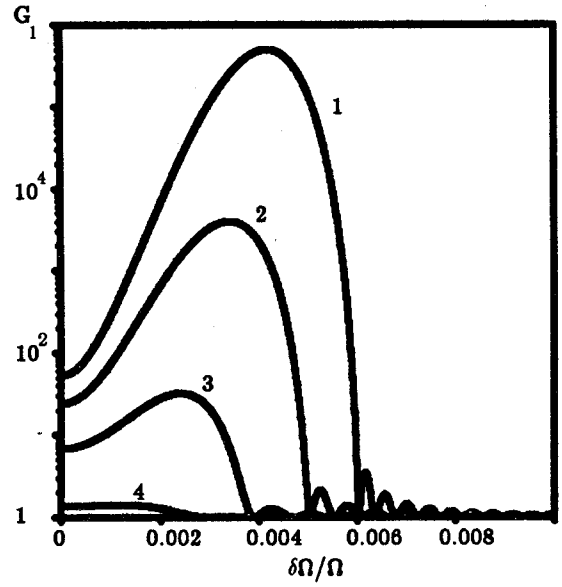

Figure 6. Amplification G_1 of the probe wave versus frequency modulation index $\delta\Omega/\Omega$ for the case of a 1 km long Ge-doped silica fiber. (Curves: 1 – 60% of instability threshold p_{cr} [120 times of the amplification threshold, I_{amp}], 2 – 40% of p_{cr} [80× of I_{amp}], 3 – 20% of p_{cr} [40 × of I_{amp}], and 4 – 5% of p_{cr} [10 × of I_{amp}]).

We define the intensity amplification G_1 for the probe wave $A_{1,1}$, as: $G_1 = |A_{1,1}(\xi=1)/A_{1,1}(\xi=0)|^2$. The variation of G_1 versus normalized frequency detuning $\delta\Omega$ is depicted in Figs. 6 for the 1 km long Ge-doped silica fiber in Section 3 with pumping at 60%, 40%, 20%, and 5% of the threshold intensity $I_{cr} = 9.3 MW/cm^2$. One can see that even when the pumping is well below the threshold of instability, the bandwidth and amplification are still appreciable. For instance, in the case of pumping at 20% of the threshold of instability the gain $\simeq 20$ and bandwidth $\simeq 2.5\times10^6$ (7.4×10^{11} Hz or 0.4% of the pumping frequency). Unlike the "artificial" case with large dispersion d and near-threshold pumping [7], the gain spectra in Fig. 6 are smooth, i.e. no pronounced resonances are present.

We found [7] that for $d \ll 1$, the gain G_1 can be represented approximately as:

$$G_1 \simeq \begin{cases} 1 + p^2 + 2(1+p^2/3)\,|dp|\,\delta\Omega^2 & \text{for } \delta\Omega \ll (\delta\Omega)_o \\ \dfrac{exp\left(2\delta\Omega[2\,|dp|-(d\delta\Omega)^2]^{1/2}\right)}{|D(\lambda=i\delta\Omega,p,d)|^2} & \text{for } \delta\Omega > (\delta\Omega)_o \end{cases} \quad (5)$$

where $(\delta\Omega)_o = (8\,|pd|)^{-1/2}\ln(1+p^2)$, D is the determinant defining the threshold of instability [7]. Eq. (5) correctly predicts that the gain slowly raise from p^2+1, its value at $\delta\Omega=0$, when $\delta\Omega < (\delta\Omega)_o$. This portion of the gain spectrum for $\delta\Omega \ll (\delta\Omega)_o$ corresponds to the contribution from dispersionless four wave mixing [19]. Beyond $(\delta\Omega)_o$, the variation of gain obeys $\sim\exp(2\delta\Omega[2\,|dp|-(d\delta\Omega)^2]^{1/2})$ when pumping power $|p|$ is substantially below p_{cr}. This part of the gain is solely caused by dispersion-related process. The determinant D, which is equal to one in most conditions [7] (especially in the realistic situation when $|d| \ll 1$) except at near-threshold pumping, is responsible for the resonant modes and instability.

From Eq. (5), we note that a nonzero amplification (or $G_1 > 0$) can be obtained for any pumping intensity, however, for each fixed intensity $|p|$, the frequency detuning should be smaller than certain cutoff frequency, $(\delta\Omega)_{cr}$,

$$|\delta\Omega| \le (\delta\Omega)_{cr} \simeq \sqrt{2\,|p/d|}\,. \quad (6)$$

Therefore, a rough estimate of the amplification bandwidth is given by $(\delta\Omega)_{cr}$, Eq. (6), which is valid for arbitrary pumping, $|p| < p_{cr}$. The maximum bandwidth $(\delta\Omega)_{max}$ for a fixed dispersion d is attained when $|p| = p_{cr}$, Eq. (4), i.e.

$$(\delta\Omega)_{max} \simeq \sqrt{2\,|log_\eta\,|d|/d|}\,. \quad (7)$$

The location of the peak gain $(\delta\Omega)_{opt}$, i.e. the frequency of the mode with lowest threshold of instability, can be approximately estimated as:

$$(\delta\Omega)_{opt} = (\delta\Omega)_{cr}/\sqrt{2} \quad (8)$$

The results from these approximate equations for frequency, Eqs. (6) - (8), are qualitatively close to the exact values from numerical calculation shown in Fig. 6.

The results above indicate that the nonlinear fiber with dispersion, pumped by counterpropagating waves has great potential as an all-optical amplifier operating in cw or quasi-cw regime which may find application in optical gyroscopes, optical fiber communications, etc. One possible limiting factor in amplification is the losses in the fiber which have not been included in our calculation. To estimate the effect of losses in the optical fiber, we introduce a threshold intensity of amplification I_{amp}, which satisfies the following condition:

$$\alpha L = \Gamma(I_{amp}) \quad (9)$$

where α is the loss coefficient and $\Gamma(I_{amp}) = \ln[G_1(I_{amp})]$ is the growth rate at the amplification threshold in the lossless approximation, i.e. the gain must be equal to loss at I_{amp}. Substituting Eqs. (5), (6) and (8) into Eq. (9), we

obtain a remarkably simple expression for I_{amp} at $(\delta\Omega)_{opt}$:

$$I_{amp} = \alpha/(2n_2k) \qquad (10)$$

which does not depend on either length or dispersion. For the silica fiber considered in Section 5, $\alpha = 0.5dB/km = 0.12\,km^{-1}$ [15] and $n_2k = 1.3\times10^{-6}\,km^{-1}$ [16]. Hence, the threshold of amplification is $46.2kW/cm^2$ (or 0.5% of the threshold of instability in the example with $L = 1km$ and $\mu = 14psec/nm-km$). For a typical fiber with effective area of 50 μm^2 [15],[16] the threshold pumping power for amplification is 23mW. This excellent performance is attributed to the low loss in the fiber.

5. Conclusion

In conclusion, we showed that linear frequency dispersion together with Kerr nonlinearity can result in amplification and temporal instability of nonlinear counterpropagating waves. As the pumping increases above certain threshold, self-oscillations are excited; upon further increase of pumping they evolve into subharmonics and chaos. With under-threshold pumping, large gain and broad-band amplification are to be found. The mechanism of the entire phenomenon can be explained in terms of positive distributed feedback from the nonlinear index grating formed by the two laser beams. Our calculations show that the amplifiers based on the nonlinear optical fiber pumped by counterpropagating waves with relatively low power have great potential for various applications.

Acknowledgements

This research is supported by AFOSR; the numerical results are obtained using Cray-YMP at Pittsburgh Supercomputing Center.

References

1. H. G. Winful and J. H. Marburger, Appl. Phys. Lett. 36, 613 (1980).
2. A. E. Kaplan, Opt. Lett. 8, 560 (1983).
3. A. E. Kaplan and C. T. Law, IEEE J. Quant. Elect. 21, 1529 (1985).
4. A. L. Gaeta, R. W Boyd, J. R. Ackerhalt and P. W. Milonni, Phys. Rev. Lett. 58, 2432 (1987); G. Khitrova, J. F. Valley, and H. M. Gibbs, Phys, Rev. Lett. 60, 1126 (1988). D. J. Gauthier, M. S. Malcuit and R. W. Boyd, Phys. Rev. Lett. 61, 1827 (1988).
5. J. Yumoto and K. Otsuka, Phys. Rev. Lett. 54, 1806 (1985); M. V. Tratnik and J. E. Sipe, Phys. Rev. A35, 2965 (1987).
6. I. Bar-Joseph and Y. Silberberg, Phys. Rev. A36, 1731 (1987); Y. Silberberg and I. Bar-Joseph, Phys. Rev. Lett. 48, 1541 (1982) and J. Opt. Soc. Am. B1, 662 (1984).
7. C. T. Law and A. E. Kaplan, Opt. Lett. 14, 734 (1989); C. T. Law and A. E. Kaplan, "Instabilities and amplification of counterpropagating waves in a Kerr nonlinear medium," to appear in J. Opt. Soc. Am. B.
8. S. A. Akhmanov, R. V. Khokhlov, and A. P. Sukhorukov, in Laser Handbook, ed. F. T. Arecchi and E. O. Schulz-Due Bois (North Holland, Amsterdam, 1972).
9. V. E. Zakharov and A. B. Shabat, Sov. Phys. JETP 34, 62 (1972); A. Hasegawa and F. Tappert, Appl. Phys. Lett. 23, 142 (1973); A. Hasegawa and F. Tappert, Appl. Phys. Lett. 142 (1973).
10. G. P. Agrawal, Phys. Rev. Lett. 59, 880 (1987).
11. C. Pare, M. Piche and P.-A. Belanger, J. Opt. Soc. Am B5, 676 (1988).
12. A. E. Kaplan and P. Meystre, Opt. Lett 6, 590 (1981) and Opt. Commun. 40, 229 (1982); R. A. Bergh, H. C. Lefevre, and H. J. Shaw, Opt. Lett. 7, 282 (1982); S. Ezekiel, J. L. Davis, and R. W. Hellwarth, Opt. Lett. 7, 457 (1982).
13. J. E. Bjorkholm, P. W. Smith, W. J. Tomlinson, and A. E. Kaplan, Opt. Lett. 6, 345 (1981); A. E. Kaplan, Opt. Lett. 6, 360 (1981).
14. W. J. Firth and C. Pare, Opt. Lett., 13, 1096 (1988).
15. J. W. Fleming, J. Am. Ceram. So. 59, 503 (1976); T. Li, IEEE Trans. Comm. COM-26, 946 (1978).
16. R. Hellwarth, J. Cherlow and T. T. Yang, Phys. Rev. B11, 964 (1975); R. H. Stolen, in Optical Fiber Telecommunications, ed. S. E. Miller and A. G. Chynoweth (Academic Press, New York, 1979), p. 125; R. G. Smith, Appl. Opt. 11, 2489 (1972).
17. S. R. Friberg and P. W. Smith, IEEE J. of Quant. Elect. QE-23, 2089 (1987).
18. J. H. Marburger, in Optical Phase Conjugation, R. A. Fisher, ed. (Academic, New York 1982), p. 99.
19. D. M. Pepper and A. Yariv, in Optical Phase Conjugation, R. A. Fisher, ed. (Academic, New York 1982), p. 24.